



Identification of the heart wall and chamber based on temporal change of ultrasonic scatterer distribution

Kohei Takahashi¹, Hirofumi Taki^{1,2}, and Hiroshi Kanai^{2,1*}

¹Graduate School of Biomedical Engineering, Tohoku University, Sendai 980-8579, Japan

²Graduate School of Engineering, Tohoku University, Sendai 980-8579, Japan

*E-mail: kanai@ecei.tohoku.ac.jp

Received November 24, 2016; accepted March 6, 2017; published online June 12, 2017

In most current methods for evaluating the cardiac function by ultrasound, the heart wall area is identified manually by an examiner. To eliminate examiner dependence and to improve usability, an automatic heart wall identification method is desirable. Identification based on only echogenicity often fails because of low echogenicity of some areas of the heart wall. In the present study, to determine more essential features, we focused on the relative temporal change of ultrasonic scatterer distribution and proposed three features for identification of the heart wall and the chamber: cross-correlation of RF signals, that of envelopes, and spatial dispersion of movement vectors in small regions. In an *in vivo* experiment, using echogenicity and the three features, we identified the heart wall and the chamber in the left ventricular long-axis view, resulting in criteria of separability J of 1.69, 1.40, and 3.02 using these features compared with the result of 0.979 using echogenicity.

© 2017 The Japan Society of Applied Physics

1. Introduction

Echocardiography is useful for the screening of diseases because of its noninvasiveness, low cost, and repeated applicability.¹⁻³⁾ In addition, quantitative evaluation of myocardial function by ultrasound has been developed for the early detection of cardiac diseases. For example, ultrasound Doppler measurements with high temporal resolution have been developed to evaluate intracardiac blood flow⁴⁾ and cardiac wall motion.⁵⁾ Methods of evaluating two-dimensional cardiac wall motion and strain rate by the ultrasound speckle tracking method have also been reported.⁶⁻¹²⁾ Ultrasound measurement with high temporal resolution also enables imaging of the vibration propagation caused by closure of the heart valve and contractile response by electrical excitation.¹²⁻¹⁵⁾

In most of these methods, the heart wall area, which is the object to be analyzed, is manually identified in a cross-sectional image of the heart. Alternatively, to eliminate examiner-dependence and to improve usability, an automatic heart wall identification method is strongly desired. Several researchers have proposed automatic or semi-automatic identification methods using echogenicity to distinguish regions of the heart wall from the chamber.¹⁶⁻¹⁸⁾ However, the echogenicity of the heart wall changes owing to temporal variation of the direction of the myocardial fiber¹⁹⁾ and the mismatch of acoustic impedance,²⁰⁾ sometimes resulting in the appearance of hypogenic areas in the heart wall during a cardiac cycle. Therefore, high-accuracy identification of the heart wall based on only echogenicity is difficult.

As a solution to this problem, some identification methods using features other than echogenicity have been developed. These methods use not only the information in each frame but also the information of consecutive frames. Dydenko et al. proposed a boundary detection method utilizing the difference of velocity between that in the heart wall and that in the chamber.²¹⁾ Other researchers have proposed identification methods utilizing the differences of cross-correlation of the received signals between frames, resulting in improvement of the identification of the heart wall in ejection and filling phases.^{22,23)} For identification of the heart wall and the

chamber, Kinugawa et al. proposed using the magnitude-squared coherence (MSC) function, which evaluates the variance of the phase shift of the radio frequency (RF) signals between consecutive frames.²⁴⁾ Takahashi and Nakahara et al. proposed a method utilizing echogenicity and MSC, which improved results of identification in the slow filling phase.²⁵⁻²⁷⁾ These methods showed the effectiveness of features other than echogenicity for identification. Achievement of high-accuracy identification, however, has been restricted to the cardiac phase: the transition period from the rapid filling phase to the slow filling phase, which is relatively easy to identify. Herein, more essential features for differentiation of the heart wall from the chamber during a cardiac cycle are proposed.

2. Principle

A method to identify the heart wall and the chamber which focuses on the temporal change of scatterer spatial distribution is herein proposed as follows.

2.1 Temporal change of scatterer spatial distribution

In the heart wall, major scatterers are intercellular substances consisting of collagen fibers. These scatterers exist between myocardial bundles, and the solid structure of these bundles maintains the scatterer spatial distribution. In the chamber, on the other hand, major scatterers are red blood cells. Figure 1 shows a schema of temporal change of scatterer spatial distribution in the heart wall and the chamber. The heart wall has translational motion^{28,29)} corresponding to contraction and relaxation and motion which is caused by the change in thickness.⁷⁻¹¹⁾ Translational motion shifts RF signals to the direction of the motion, and thickness change causes temporal changes of the RF signal waveforms because scatterer spatial distribution change. The shift of RF signals, caused by translational motion can be canceled by the tracking method described below, and it can be assumed that the change in thickness during a short time period is minute. In addition, in the left ventricular long-axis view, scatterers in the heart wall mainly move in the axial direction not in the lateral and elevational directions. The axial direction can be followed by tracking the heart wall because the tracking method employed in the present study

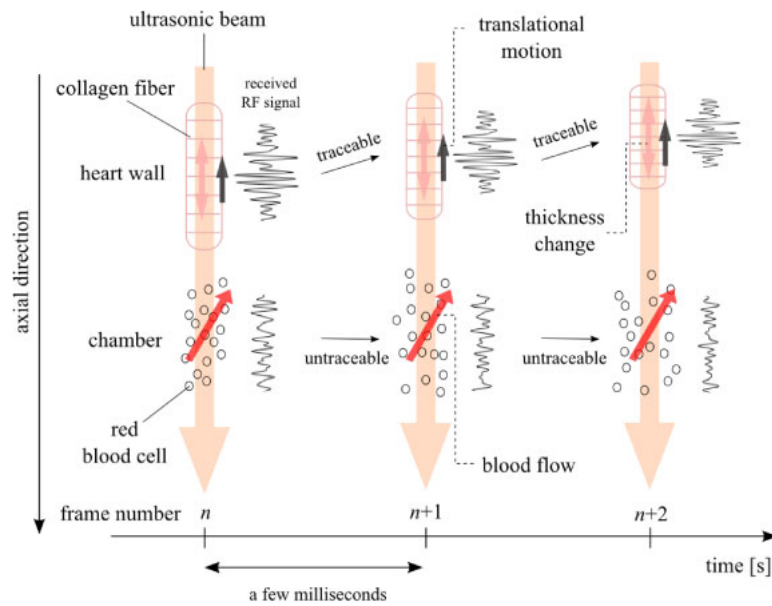


Fig. 1. (Color online) Illustration of temporal change of scatterer distribution and RF signals.

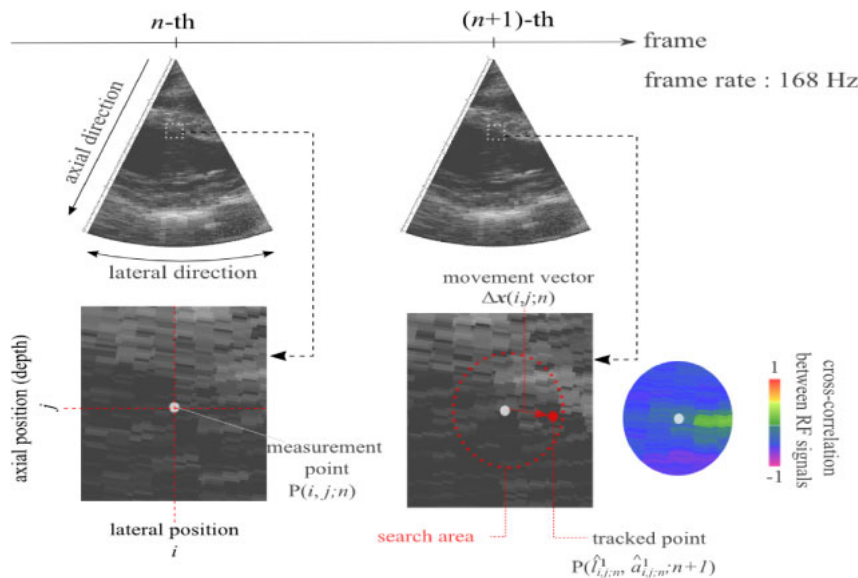


Fig. 2. (Color online) Illustration of tracking method.

is highly accurate in estimating axial movement of the heart wall.

In the chamber, on the other hand, blood motion causes large temporal changes in the RF signal waveforms because the scatterer spatial distribution changes. The blood flow causes red blood cell scatterers in the chamber to move in lateral, axial, and elevational directions.³⁰ Thus, the relative temporal change of scatterer spatial distribution in the chamber should be sufficiently larger than that in the heart wall when tracking is applied to the heart wall. Therefore, temporal change of RF signal waveforms in the consecutive frames is suitable for differentiating the heart wall from the chamber.

2.2 Tracking method

Figure 2 shows the tracking method employed in the present study. As shown in the figure, $P(i, j; n)$ denotes the measurement point at lateral position i and axial position j in the n -th frame. The movement of each point $P(i, j; n)$ is

estimated from the cross-correlation between RF signals of consecutive frames in the search area, which is set within a circle centered on $P(i, j; n)$ to be tracked. Moreover, $P(\hat{l}_{i,j;n}^k, \hat{a}_{i,j;n}^k; n+k)$ denotes the estimated point of $P(i, j; n)$ in the $(n+k)$ -th frame by the tracking method, where $\hat{l}_{i,j;n}^k$ and $\hat{a}_{i,j;n}^k$ respectively show the estimated lateral and axial positions at k frames after the point $P(i, j; n)$ set at n -th frame. The displacement of the measurement point $P(i, j; n)$ from the n -th frame to the $(n+1)$ -th frame is described as movement vector $\Delta x(i, j; n)$, which is defined as follows:

$$\Delta x(i, j; n) = P(\hat{l}_{i,j;n}^1, \hat{a}_{i,j;n}^1; n+1) - P(\hat{l}_{i,j;n}^0, \hat{a}_{i,j;n}^0; n), \quad (1)$$

where $P(\hat{l}_{i,j;n}^0, \hat{a}_{i,j;n}^0; n)$ is equivalent to $P(i, j; n)$.

The tracking method calculates two-dimensional cross-correlation in a cross-sectional image with lateral and axial directions and is able to cancel the translational motions both in the axial and lateral directions. Moreover, the translational motion in elevational direction can be neglected in the

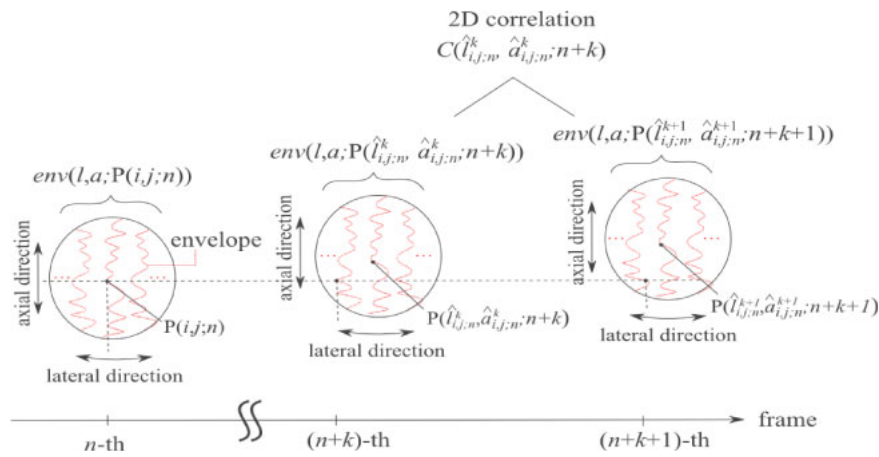


Fig. 3. (Color online) Illustration of envelopes in a small circular region.

present study, as described below. An acquired cross-sectional image has a thickness in the elevational direction that is equivalent to the beam width in the direction of the sector probe to be used. By increasing the frame rate so that the maximum displacement of the heart wall between consecutive frames is sufficiently smaller than the beam width in elevational direction, the same regions of the heart wall are included in cross-sectional images of consecutive frames. Therefore, the translational motion in the elevational direction is neglected, and the motions both in axial and lateral directions can be cancelled by the tracking method.

2.3 Features for identification

In the present study, for identification of the heart wall and the chamber, the following three features were introduced, all of which reflect the differences between the heart wall and the chamber in the small circular region between consecutive frames.

2.3.1 Cross-correlations of RF signals and envelopes between consecutive frames.

As illustrated in Fig. 1, the temporal change of RF signal waveforms in the chamber is sufficiently larger than that in the heart wall. To detect the temporal change of RF signals, a cross-correlation technique was applied to the RF signal and those envelopes after the tracking process. The RF signals can evaluate the change of waveforms more accurately by phase information when tissue deformation is sufficiently small. On the other hand, the envelopes of the RF signals have the advantage of being robust against the change of the RF waveforms when tissue deformation is large. According to the cross-correlation error regarding the RF signals and those envelopes with tissue deformation, RF signals have fewer errors than envelopes when tissue deformation is under 0.1%, and envelopes have fewer errors than RF signals when tissue deformation is over 2%.³¹⁾ Therefore, in the present study, both cross-correlations are employed as follows.

A set of the envelope signals within a small circular region centered on the point $P(\hat{l}_{i,j;n}^k, \hat{a}_{i,j;n}^k; n+k)$ is defined as $env(l, a; P(\hat{l}_{i,j;n}^k, \hat{a}_{i,j;n}^k; n+k))$, as shown Fig. 3. Let us define the two-dimensional cross-correlation value $C_{env}(\hat{l}_{i,j;n}^k, \hat{a}_{i,j;n}^k; n+k)$ with zero lag of the set of envelope signals within a small circular region centered on the tracked point $P(\hat{l}_{i,j;n}^k, \hat{a}_{i,j;n}^k; n+k)$ between two consecutive frames from the $(n+k)$ -th frame by

$$C_{env}(\hat{l}_{i,j;n}^k, \hat{a}_{i,j;n}^k; n+k) = \text{corr}\{env(l, a; P(\hat{l}_{i,j;n}^k, \hat{a}_{i,j;n}^k; n+k)), env(l, a; P(\hat{l}_{i,j;n}^{k+1}, \hat{a}_{i,j;n}^{k+1}; n+k+1))\}, \quad (2)$$

where $\text{corr}\{\dots\}$ is the two-dimensional cross-correlation function with zero lag. Moreover, the temporal average $C_{env,ave}(i, j; n)$ of $C_{env}(\hat{l}_{i,j;n}^k, \hat{a}_{i,j;n}^k; n+k)$ among consecutive $2N$ frames is applied as follows:

$$C_{env,ave}(i, j; n) = \frac{\sum_{k=-N}^{N-1} [C_{env}(\hat{l}_{i,j;n}^k, \hat{a}_{i,j;n}^k; n+k) \times w(k)]}{\sum_{k=-N}^{N-1} w(k)}, \quad (3)$$

where $w(k)$ is a Hanning window function with a length of $2N$. The averaged cross-correlation $C_{RF,ave}(i, j; n)$ of the RF signals between consecutive frames is calculated in the same way as the calculation of $C_{env,ave}(i, j; n)$.

2.3.2 Dispersion of movement vectors.

By applying the tracking method, displacement between consecutive frames is estimated as movement vector $\Delta\mathbf{x}(i, j; n)$ for every discrete point $P(i, j; n)$. As illustrated in Fig. 4(a), the movement vector $\Delta\mathbf{x}(i, j; n)$ at each point in a small circular region around $P(i, j; n)$ in the heart wall can be assumed to have similar components. In the chamber, however, the movement vector at each point in a small circular region around $P(i, j; n)$ has incoherent components because the same regions cannot be tracked due to the change in the scatterer spatial distribution. These phenomena are also valid in one-dimensional space in the axial direction, as shown in Fig. 4(b).

Let us define the movement vectors in the axial direction within a small circular region centered on the point $P(i, j; n)$ as $\text{vec}(l, a; P(i, j; n))$. To detect dispersion of the movement vectors $\text{vec}(l, a; P(i, j; n))$ in the axial direction, let us calculate their standard deviations within a small circular region. The spatial standard deviation $SD(\hat{l}_{i,j;n}^k, \hat{a}_{i,j;n}^k; n+k)$ of $\text{vec}(l, a; P(\hat{l}_{i,j;n}^k, \hat{a}_{i,j;n}^k; n+k))$ in the $(n+k)$ -th frame is defined as follows:

$$SD(\hat{l}_{i,j;n}^k, \hat{a}_{i,j;n}^k; n+k) = SD\{\text{vec}(l, a; P(\hat{l}_{i,j;n}^k, \hat{a}_{i,j;n}^k; n+k))\}, \quad (4)$$

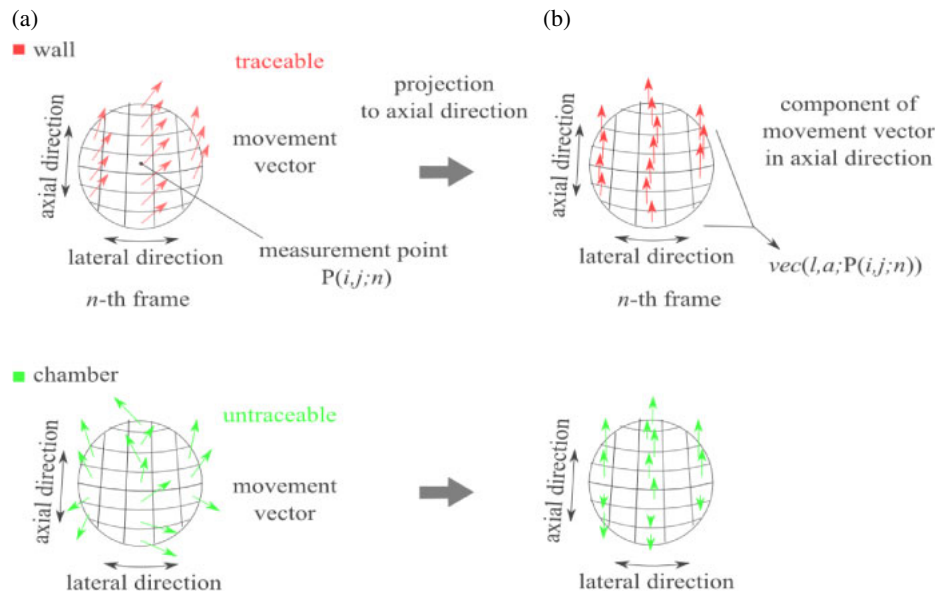


Fig. 4. (Color online) Illustration of movement vectors in a small circular region: (a) Lateral and axial directions. (b) Axial direction.

where $SD\{\dots\}$ is the function calculating the standard deviation. The temporal average $SD_{ave}(i,j;n)$ of $\{SD(\hat{l}_{i,j;n}^k, \hat{a}_{i,j;n}^k; n+k)\}$ among consecutive $2N$ frames is defined as follows:

$$SD_{ave}(i,j;n) = \frac{\sum_{k=-N}^{N-1} [SD(\hat{l}_{i,j;n}^k, \hat{a}_{i,j;n}^k; n+k) \times w(k)]}{\sum_{k=-N}^{N-1} w(k)}. \quad (5)$$

These features of $C_{env,ave}(i,j;n)$, $C_{env,ave}(i,j;n)$, and $SD_{ave}(i,j;n)$ were employed to identify the heart wall and the chamber as described in the next section.

2.4 Automatic identification of heart wall and chamber

In the present study, the automatic method for identification of the heart wall and the chamber was employed.²⁷⁾ At the beginning, in order to reduce the clutter component from the surrounding tissue, a moving target indicator (MTI) filter for RF signals was applied as a high-pass filter, its cut-off frequency being 10 Hz.^{26,32)} After MTI filtering, the features described above were calculated at all discrete points in all frames and were spatially smoothed by adaptive mean (AM) filtering.^{33,34)} By the expectation-maximization (EM) algorithm,³⁵⁾ we classified the heart wall and chamber automatically and identified the areas of all frames in a cardiac cycle. Using the EM algorithm, a mixture of two Gaussian distributions, which correspond to the heart wall and the chamber, was fitted to the features of all discrete points in a frame. The threshold for the classification of each data point was determined where the two probabilities of the determined Gaussian distributions had the same value.

In order to compare the classification accuracy of the proposed method with that of the conventional method using echogenicity, criterion J of separability was introduced as a function to evaluate classification accuracy.³⁶⁾ By identifying the interventricular septum (IVS) and the left ventricle (LV) manually, classification accuracy between the two areas was evaluated. Using the feature at each measurement point in

the IVS and the LV, the interclass covariance S_B , which corresponds to the distance between means of classes was calculated, as was intraclass covariance S_W , which corresponds to the mean variance of features within classes. Separability of the feature increased in proportion to the distance between means of classes, whereas it decreased in proportion to the variances of features within classes. Therefore, criterion J of separability was defined by normalizing the interclass covariance S_B by the intraclass covariance S_W as follows:

$$J = \frac{S_B}{S_W}. \quad (6)$$

2.5 In vivo measurement

In the present study, the heart of a healthy human subject was measured in the left ventricular long-axis view during a cardiac cycle (center frequency: 3.5 MHz; frame rate: 168 Hz; sampling frequency: 20 MHz). The measurement intervals in the axial and time directions were 38.5 μm and 5.95 ms, respectively, and the measurement interval in the lateral direction was 3.99 mm at the center position of the region of interest (ROI). The -12 dB width of the ultrasonic beam pulse was 0.50 mm, and that of the ultrasonic beam was 9.0 mm, 12 mm in lateral and elevational directions, respectively. Since the maximum velocity of the heart wall is less than 0.1 m/s,³⁷⁾ the maximum displacement of the heart wall between consecutive frames by translational motion is approximately 595 μm when the frame rate is 168 Hz. Therefore, the radius of the search area for the tracking method was set at 595 μm . The translational motion in elevational direction of the heart wall could be neglected because the maximum displacement of the heart wall between consecutive frames was sufficiently smaller than the width of ultrasonic beam in the elevational direction. For calculating the average cross-correlation of envelopes of Eq. (3) and average dispersion of movement vectors of Eq. (5), the radius of the small region and the number of frames $2N$ were set at 1.8 mm and 18 frames, respectively.

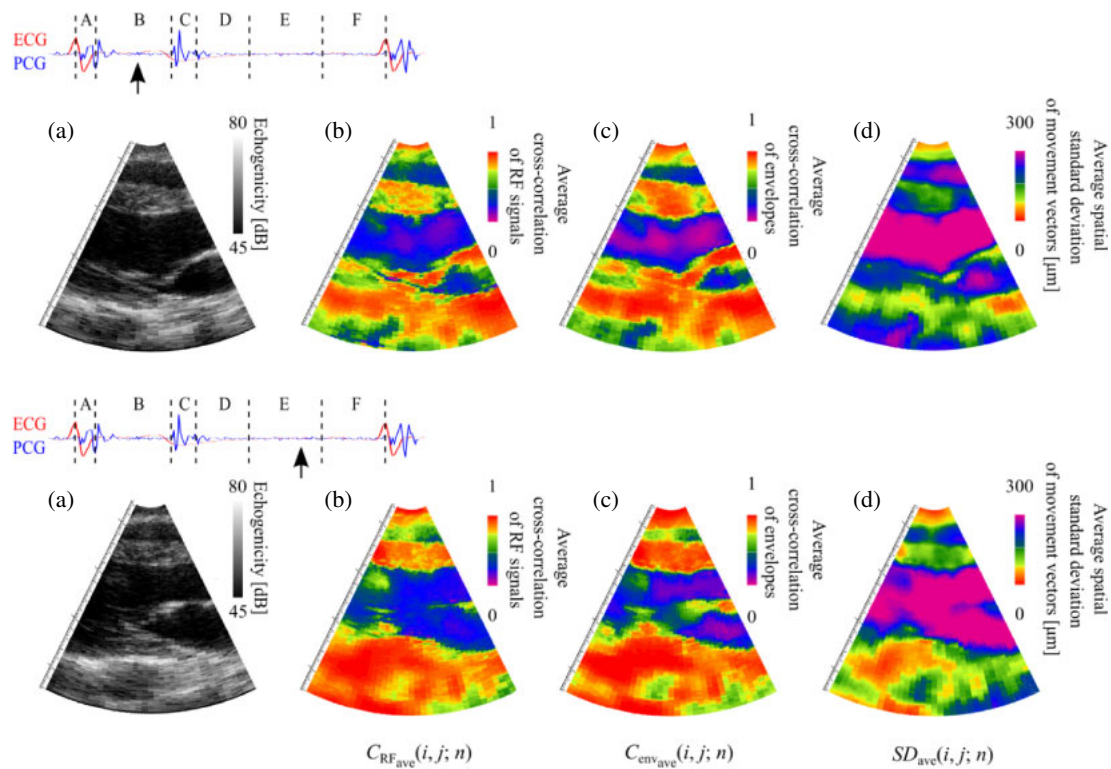


Fig. 5. (Color online) Two images of left ventricular long-axis view: (a) B-mode image. (b) Average cross-correlation of RF signals. (c) Average cross-correlation of envelopes. (d) Average spatial standard deviation of movement vectors. Periods A, B, C, D, E, and F denote the isovolumetric contraction phase, the ejection phase, the isovolumetric relaxation phase, the rapid filling phase, the slow filling phase, and the atrial systole phase, respectively.

3. Results and discussion

3.1 Effectiveness of the proposed features for identification

Figure 5 shows the B-mode image and color mapping images of each of the three features for two typical phases during a cardiac cycle. The average cross-correlations, $C_{RF,ave}(i, j; n)$ of RF signals and $C_{env,ave}(i, j; n)$ of envelopes between consecutive frames, and the average spatial standard deviation $SD_{ave}(i, j; n)$ between movement vectors mostly have large and small values, respectively, in the area with high echogenicity but mostly have small and large values, respectively, in the area with low echogenicity. These results show the effectiveness of the proposed features for identification of the heart wall and the chamber. However, in the color mapping images of these three features, the blue/purple areas, i.e., the areas with low cross-correlation value or high deviation value, are shown in the heart wall. In the color mapping of $C_{RF,ave}(i, j; n)$ and $C_{env,ave}(i, j; n)$, the green/yellow areas, i.e., the areas with high cross-correlation value, are shown in the chamber. The former areas are caused by the change in thickness of the heart wall, and the latter areas are caused by artifacts, which cannot be removed by MTI filtering. Also in the B-mode images, areas with low and high echogenicity are seen in the heart wall and the chamber, respectively. The influence of these areas on the identification is evaluated quantitatively in the next section.

Furthermore, the valves in color mapping are not as sharp as those in B-mode images. This would be caused by error in tracking of the valves. In the present study, the radius of the search area was set at $595 \mu\text{m}$ to track the heart wall in the consecutive frames. It is difficult to track the valves because

the velocity of the valve is much larger than that of the heart wall. However, as shown in Fig. 5, since the valve is sufficiently clear in the B-mode image, it is not considered to be a subject for identification in the present study.

Figure 6 shows the temporal changes of features during a cardiac cycle in three areas, the definite and indefinite areas of the IVS, i.e., IVS with high and low echogenicity, and the areas of the LV. Periods A, B, C, D, E, and F denote the isovolumetric contraction phase, the ejection phase, the isovolumetric relaxation phase, the rapid filling phase, the slow filling phase and the atrial systole phase, respectively. The echogenicity of the indefinite areas of the IVS was close to that of the LV during the latter half of period B to E. On the other hand, the average cross-correlations $C_{RF,ave}(i, j; n)$ of RF signals and $C_{env,ave}(i, j; n)$ of envelopes and the average spatial standard deviation $SD_{ave}(i, j; n)$ of the movement vector of the indefinite areas of the IVS were close to those of the LV only during the period from the latter half of period B to the former half of the period D. These results show the effectiveness of the proposed features in distinguishing indefinite areas of the IVS from LV, and also show the possibility of more accurate identification of the heart wall and the chamber than obtainable with the echogenicity.

3.2 Identification results using proposed features

Figure 7 shows the temporal change of criterion J of separability at the time of identification by using echogenicity, the average cross-correlation of RF signals, the average cross-correlation of envelopes, and the average spatial standard deviation of the movement vectors. Table I shows the mean and the standard deviation during a cardiac cycle. The identification result using the average spatial standard deviation of movement vectors achieved the best

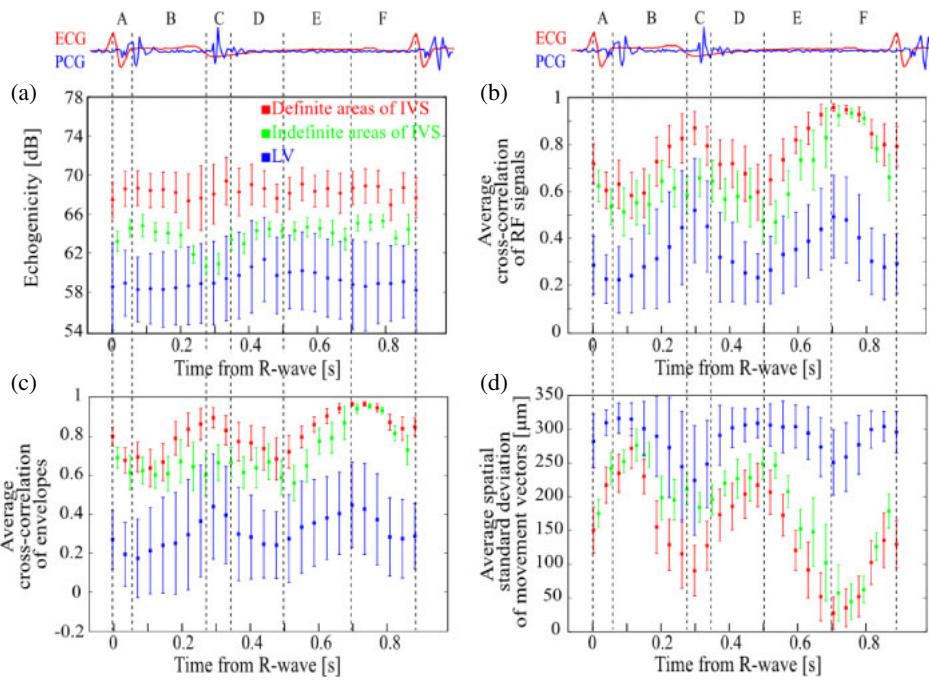


Fig. 6. (Color online) Temporal changes of features in three areas. (a) Echogenicity. (b) Average cross-correlation of RF signals. (c) Average cross-correlation of envelopes. (d) Average spatial standard deviation of movement vectors. Red, green, and blue lines denote the definite areas of the IVS, indefinite areas of the IVS, and the LV, respectively. Periods A, B, C, D, E, and F denote the isovolumetric contraction phase, the ejection phase, the isovolumetric relaxation phase, the rapid filling phase, the slow filling phase, and the atrial systole phase, respectively.

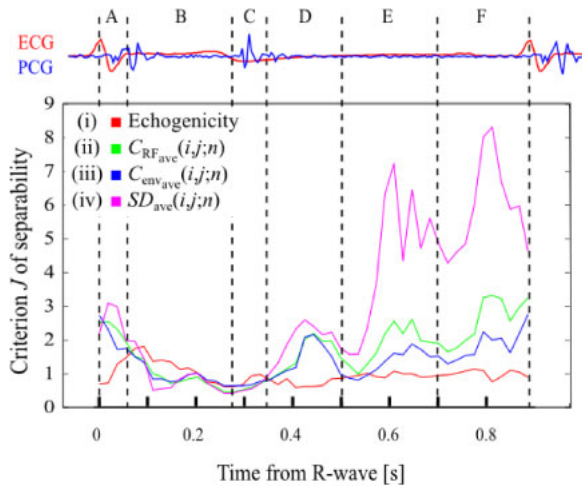


Fig. 7. (Color online) Temporal changes of criterion J of separability. Results of identification using (i) echogenicity, (ii) average cross-correlation of RF signals, (iii) average cross-correlation of envelopes, and (iv) average spatial standard deviation of movement vectors. Periods A, B, C, D, E, and F denote the isovolumetric contraction phase, the ejection phase, the isovolumetric relaxation phase, the rapid filling phase, the slow filling phase, and the atrial systole phase, respectively.

performance, i.e., $J = 3.02 \pm 2.27$, and the result using cross-correlation of RF signals and envelopes achieved a comparable performance of $J = 1.69 \pm 0.842$ and 1.40 ± 0.577 . Particularly during the whole periods A, C, E and F, criterion J of separability using the proposed features was higher than that using echogenicity, which the conventional identification method was based on. As described in the previous section, in the color mapping images of Fig. 5, blue/purple and green/yellow areas are respectively seen in the heart wall and the chamber, and in the B-mode images, areas with low and high echogenicity are respectively seen

Table I. Criterion J of separability during a cardiac cycle, evaluated for (i) echogenicity, (ii) the average cross-correlation of RF signals, (iii) the average cross-correlation of envelopes, and (iv) the average spatial standard deviation of movement vectors.

(i)	(ii)	(iii)	(iv)
0.979 ± 0.276	1.69 ± 0.842	1.40 ± 0.577	2.16 ± 0.455

in the heart wall and chamber. However, by quantitative evaluation using criterion J of separability as described above, it is shown that the proposed three features have a smaller influence on accurate identification than the echogenicity. Since criterion J of separability reflects the classification accuracy, the feature with high value of J can possibly enable accurate identification, comparable to manual identification by examiner. Therefore, the results show the effectiveness of identification using the proposed features.

However, temporal changes of criterion J of separability using the proposed features are larger than that using echogenicity, and criterion J of separability using the proposed features is smaller than that using echogenicity during the first half of period B. This would be caused by the temporal changes of the proposed features. In order to achieve more stable identification during a cardiac cycle, it is necessary to develop features with low temporal change by optimization of the parameters of the calculated features, i.e., the radius of the small region and the number of frames. In addition, in order to show the possibility of clinical usage, it is necessary to confirm the efficiency of the proposed method by applying it to more test subjects.

4. Conclusions

In the present study, we focused on the relative temporal changes of scatterer spatial distribution and proposed

effective features for identification of the heart wall and chamber. The identification results using the proposed features achieved criteria J of separability 1.69, 1.40, and 3.02 compared with the result of 0.979 using echogenicity. The results show the high potential of the proposed features in identifying the heart wall and the chamber.

- 1) Y. Mochizuki, H. Taki, and H. Kanai, *Jpn. J. Appl. Phys.* **55**, 07KF13 (2016).
- 2) Y. Sakai, H. Taki, and H. Kanai, *Jpn. J. Appl. Phys.* **55**, 07KF11 (2016).
- 3) Y. Kurokawa, H. Taki, and H. Kanai, *Jpn. J. Appl. Phys.* **55**, 07KF12 (2016).
- 4) W. N. McDicken, G. R. Sutherland, C. M. Moran, and L. N. Gordon, *Ultrasound Med. Biol.* **18**, 651 (1992).
- 5) G. R. Sutherland, G. D. Salvo, P. Claus, J. D'hooge, and B. Bijmens, *J. Am. Soc. Echocardiogr.* **17**, 788 (2004).
- 6) L. N. Bohs, B. J. Geinman, M. E. Anderson, S. C. Gebhart, and G. E. Trahey, *Ultrasonics* **38**, 369 (2000).
- 7) K. Kaluzynski, X. Chen, S. Y. Emelianov, A. R. Skovoroda, and M. O'Donnell, *IEEE Trans. Ultrason. Ferroelectr. Freq. Control* **48**, 1111 (2001).
- 8) J. D'hooge, E. Konofagou, F. Jamal, A. Heimdal, L. Barrios, B. Bijmens, J. Thoen, F. Van der Werf, G. Sutherland, and P. Suetens, *IEEE Trans. Ultrason. Ferroelectr. Freq. Control* **49**, 281 (2002).
- 9) Y. Honjo, H. Hasegawa, and H. Kanai, *Jpn. J. Appl. Phys.* **49**, 07HF14 (2010).
- 10) Y. Honjo, H. Hasegawa, and H. Kanai, *Jpn. J. Appl. Phys.* **51**, 07GF06 (2012).
- 11) H. Yoshiara, H. Hasegawa, H. Kanai, and M. Tanaka, *Jpn. J. Appl. Phys.* **46**, 4889 (2007).
- 12) H. Kanai, *Ultrasound Med. Biol.* **35**, 936 (2009).
- 13) H. Kanai, *IEEE Trans. Ultrason. Ferroelectr. Freq. Control* **52**, 1931 (2005).
- 14) H. Kanai and Y. Koiwa, *Ultrasound Med. Biol.* **27**, 481 (2001).
- 15) H. Kanai and M. Tanaka, *Jpn. J. Appl. Phys.* **50**, 07HA01 (2011).
- 16) J. A. Noble and D. Boukerroui, *IEEE Trans. Med. Imaging* **25**, 987 (2006).
- 17) K. Y. E. Leung and J. G. Bosch, *Eur. Heart J. Cardiovasc. Imaging* **11**, 97 (2010).
- 18) M. M. Nillesen, R. G. Lopata, H. J. Huisman, J. M. Thijssen, L. Kapusta, and C. L. de Korte, *Ultrasound Med. Biol.* **37**, 1409 (2011).
- 19) B. Hete and K. K. Shung, *IEEE Trans. Ultrason. Ferroelectr. Freq. Control* **40**, 354 (1993).
- 20) S. A. Wickline, L. J. Thomas, J. G. Miller, B. E. Sobel, and J. E. Perez, *J. Clin. Invest.* **76**, 2151 (1985).
- 21) I. Dydenko, D. Friboulet, J. M. Gorce, J. D'hooge, B. Bijmens, and I. E. Magnin, *Med. Image Anal.* **7**, 353 (2003).
- 22) A. E. C. M. Saris, M. M. Nillesen, R. G. P. Lopata, and C. L. Korte, *Ultrasound Med. Biol.* **40**, 596 (2014).
- 23) P. Yan, C. X. Jia, A. Sinusas, K. Thiele, M. O'Donnell, and J. S. Duncan, *Biennial Int. Conf. Inf. Proc. Medical Imaging*, 2007, p. 233.
- 24) T. Kinugawa, H. Hasegawa, and H. Kanai, *Jpn. J. Appl. Phys.* **47**, 4155 (2008).
- 25) H. Takahashi, H. Hasegawa, and H. Kanai, *Jpn. J. Appl. Phys.* **50**, 07HF16 (2011).
- 26) H. Takahashi, H. Hasegawa, and H. Kanai, *Jpn. J. Appl. Phys.* **52**, 07HF17 (2013).
- 27) K. Nakahara, H. Hasegawa, and H. Kanai, *Jpn. J. Appl. Phys.* **53**, 07KF09 (2014).
- 28) L. Kapusta, J. M. Thijssen, M. H. Cuypers, P. G. Peer, and O. Daniëls, *Ultrasound Med. Biol.* **26**, 229 (2000).
- 29) Y. Koya and I. Mizoshiri, *Denki Gakkai Ronbunshi C* **122**, 60 (2002) [in Japanese].
- 30) Y. Wang, R. Ma, G. Ding, D. Hou, Z. Li, L. Yin, and M. Zhang, *Ultrasound Med. Biol.* **42**, 744 (2016).
- 31) W. Yu, P. Yan, A. J. Sinusas, K. Thiele, and J. S. Duncan, *Med. Image Anal.* **10**, 495 (2006).
- 32) B. R. Mahafza, *Introduction to Radar Analysis* (CRC Press, Boca Raton, FL, 1998).
- 33) J. C. Bamber and C. Daft, *Ultrasonics* **24**, 41 (1986).
- 34) M. M. Nillesen, R. G. Lopata, I. H. Gerrits, L. Kapusta, H. J. Huisman, J. M. Thijssen, and C. L. de Korte, *Ultrasound Med. Biol.* **33**, 1453 (2007).
- 35) C. M. Bishop, *Pattern Recognition and Machine Learning* (Springer, Berlin, 2006).
- 36) K. Fukunaga, *Introduction to Statistical Pattern Recognition* (Academic Press, Boston, MA, 1990) 2nd ed.
- 37) M. Kowalski, T. Kukulski, F. Jamal, J. D'hooge, F. Weidemann, F. Rademakers, B. Bunens, L. Hatle, and G. R. Sutherland, *Ultrasound Med. Biol.* **27**, 1087 (2001).